energies

MDPI

Article

Research on Failure Characteristics of Electric Logistics Vehicle Powertrain Gearbox Based on Current Signal

Qian Tang [1,2], Xiong Shu [1,3,*], Jiande Wang [1], Kainan Yuan [4], Ming Zhang [3] and Honguang Zhou [1]

[1] Hunan Provincial Key Laboratory of Vehicle Power and Transmission System, Hunan Institute of Engineering, Xiangtan 411104, China; wjdhnu@hnie.edu.cn (J.W.)
[2] New Energy Vehicle Research Center, Hunan Institute of Engineering, Xiangtan 411104, China
[3] Department of Technology Research and Development, Xiangtan South Locomotive Manufacturing Co., Ltd., Xiangtan 411104, China; nfdj888@163.com
[4] China Machinery International Engineering Design & Research Institute Co., Ltd., Changsha 410019, China; ykn1972@126.com
* Correspondence: shux@hnie.edu.cn

Abstract: As a core component of the powertrain system of Electric Logistics Vehicles (ELVs), the gearbox is crucial for ensuring the reliability and stability of ELV operations. Traditional fault diagnosis methods for gearboxes primarily rely on the analysis of vibration signals during operation. This paper presents research on diagnosing gear tooth wear faults in ELV powertrains using motor current signals. Firstly, an experimental test platform was constructed based on the structural principle of the powertrain of ELV models. Subsequently, a pure electric light truck powertrain gearbox with tooth wear was tested. Time–frequency domain analysis, amplitude analysis, ANOVA analysis, kurtosis analysis, and zero−crossing points analysis were used to analyze the U−phase current of the motor connected to the gearbox to study the characteristics of the phase current of the drive motor after tooth wear. The results indicate that while the time–frequency domain characteristics of the U−phase currents are not significantly altered by tooth wear faults, the amplitude, variance, and kurtosis of the current increase with the severity of the wear. Conversely, the number of zero−crossing points decreases. These findings provide valuable insights into new methodologies for diagnosing faults in ELV powertrain systems, potentially enhancing the efficiency and effectiveness of troubleshooting processes.

Keywords: electric vehicle; powertrain; gearbox; fault diagnosis

check for updates

Citation: Tang, Q.; Shu, X.; Wang, J.; Yuan, K.; Zhang, M.; Zhou, H. Research on Failure Characteristics of Electric Logistics Vehicle Powertrain Gearbox Based on Current Signal. *Energies* **2024**, *17*, 3228. https://doi.org/10.3390/en17133228

Academic Editor: Massimiliano Renzi

Received: 31 May 2024
Revised: 27 June 2024
Accepted: 28 June 2024
Published: 1 July 2024

Copyright: © 2024 by the authors. Licensee MDPI, Basel, Switzerland. This article is an open access article distributed under the terms and conditions of the Creative Commons Attribution (CC BY) license (https://creativecommons.org/licenses/by/4.0/).

1. Introduction

Thanks to their unique feature of zero carbon emission, Electric Logistics Vehicles (ELVs) have been attracting increasing interest in recent years, but their reliability, particularly the reliability of their powertrain, is still a matter of concern today [1,2]. Once the powertrain fails, it can cause the vehicle to lose power and even endanger personal safety. How to quickly and accurately monitor the working status of an ELV's transmission system efficiently and reliably, and accurately and quickly locate its faults, is one of the hotspots in current research.

The gearbox is a critical component in the powertrain of electric vehicles (ELVs) that is subjected to significant dynamic loads during operation. According to ISO 10825, more than 20 types of failures have been defined that are classified into six main groups, and the most dominant were faults of bearings and lubrication [3]. The complex operating environment and conditions can easily lead to gear failures. If not discovered in time, the consequences could be catastrophic [3]. Therefore, research on gearbox fault diagnosis is of paramount practical importance. To rapidly and accurately diagnose gearbox faults and enhance the safety and reliability of electromechanical equipment operation, numerous studies have been conducted by scholars [3–22]. For instance, Sun et al. [5] proposed a

customized multi−wavelet method for diagnosing faults in planetary gearboxes, which was successfully employed to identify early pitting faults in gearbox gears. Yu et al. [6] proposed a data−driven diagnostic method to analyze the gearbox faults. Qian et al. [7] used a neuronal network method combined with gearbox vibration data to solve the problem of the gear displacement in gearboxes. Singh and his team [8] proposed a cross−domain fault diagnosis method for variable−speed gearboxes based on deep learning theory. Cheng et al. [9] established an autoregressive model (AR) model for each intrinsic mode function (IMF) component of the empirical mode decomposition (EMD), after which the autoregressive parameters of the model and the variance of the residuals were used as eigenvectors to establish the Mahalanobis distance discriminant function for the purpose of monitoring the operating conditions of the rolling bearings as well as for diagnosing their faults. Lei et al. [10] combined EMD with adaptive neuro−fuzzy inference systems (ANFISs) to successfully identify different faults and the fault severity of rolling bearings. Guo et al. [11] employed a combination of wavelet packet energy (WPE) and modulated signal bispectral analysis (MSB) to analyze planetary gearboxes with the objective of identifying the fault eigenfrequencies and achieving the fault diagnosis of planetary gearboxes. Hamadache et al. [12] combined wavelet transforms (WTs) with Gaussian processing (GP) to propose a novel approach to analyze the fault characteristics of the gearbox. Kong and Wang et al. [13] established an adaptive empirical wavelet transform framework for fault−related pattern extraction, achieved fault−related pattern extraction based on adaptive empirical wavelet transform, and then identified fault features from the envelope spectrum of the extracted patterns. Bajric et al. [14] used an adaptive threshold wavelet noise reduction technique, discrete wavelet transform, to diagnose tooth faults in gearboxes on the basis of noise cancellation processing of vibration signals of wind turbine gearboxes. Cui and Liu et al. [15,16] used different methods of threshold selection for bearing faults and noise reduction in vibration signals by wavelet transform. Magadán et al. [17] proposed a novel robust health prognostics technique that detects inner−race bearing failures and predicts the RUL of electric motor bearings under various motor conditions without model retraining or fine−tuning. Due to the expense of provoking faults in real scenarios to obtain data, Magadán and his team members proposed the use of the tabular prior−data fit network (TabPFN) model for the classification of faults in rotating machinery [18,19]. Milan et al. [20,21] conducted a failure analysis of gearboxes and bearings of the belt conveyors system. The characteristics of single−stage planetary and cycloidal reducers are analyzed in detail in [22], and the results show that planetary reducers have an advantage if a lower gear ratio is needed.

However, the aforementioned research on gearbox troubleshooting predominantly relies on the analysis of vibration signals generated during operational conditions. This approach requires the installation of specialized vibration sensors and the use of advanced signal acquisition equipment, which not only escalates development costs but also demands a high level of expertise from the signal collector. The reliability of the obtained signals is highly dependent on the sensor placement with significant variations in vibration signals observed at different locations. In contrast, motor current signals serve as the input source for many electromechanical devices, and faults in these devices inevitably lead to alterations in the current signals. Therefore, detecting current signals can effectively identify malfunctions in the connected devices. Moreover, most electrical equipment is already equipped with basic current and voltage sensors, making the acquisition of electrical signals considerably more cost−effective than obtaining vibration signals through specialized vibration sensors. Currently, motor current signature analysis has been successfully applied to the detection and diagnosis of motor faults in the electrical field, such as rotor short−circuit, air gap eccentricity, winding, motor bearing and other faults [23,24]. Nevertheless, the efficacy of motor current signature analysis in the monitoring and diagnosis of downstream mechanisms (e.g., gearboxes) of electromechanical machines remains under−researched [25,26]. However, Kia et al. [27] demonstrated that mechanical faults can be identified through the analysis of the signal spectrum, specifically the amplitude of the supply line frequency and

the presence of fault−characterizing sidebands. In Brav's study [28], a method based on discrete wavelet decomposition is applied to condition monitoring and the fault diagnosis of gearboxes. Gu et al. [29] proposed a method for detecting gearbox punching tooth wear faults utilizing motor current feature bispectral analysis. Chai et al. [30] employed a sparse signal decomposition method based on data envelopment and resonance for gearbox fault diagnosis. Kia et al. [31] developed a current space vector−based approach for tooth fault detection, focusing on the condition monitoring and fault diagnosis of gearboxes. Recent advancements in science, technology, and artificial intelligence have led to the widespread application of techniques such as convolutional neural networks (CNNs) [32], K−nearest neighbor (KNN) [33], Bayesian decision tree (BDT) [34], and artificial neural networks (ANN) [35] in gearbox fault diagnosis. These methodologies typically involve the extraction of fault features through time–frequency domain analysis of transmission vibration signals, which is followed by prediction using a multi−fault feature fusion approach [36]. Nevertheless, these advanced techniques demand significant computational power and extensive datasets, which presents a challenge for diagnosing gearboxes with limited sample data.

There is no doubt that the aforementioned studies make great contributions to understanding the fault diagnosis and analysis of gearboxes. However, most of the studies are based on using the collected vibration signals of the gearboxes to carry out fault analysis and diagnosis studies on them. In addition, the existing electrical signal−based transmission fault diagnosis research is mainly based on the wind turbine transmission or industrial transmission systems, which is significantly different from the electric vehicle transmission system in terms of working conditions, load characteristics and transmission system structure. In the powertrain system of the ELV model, the gearbox is directly connected to the drive motor in a coaxial series with splines. During vehicle operation, the motor controller controls the rotation of the motor and inputs torque and speed to the gearbox via a mechanical shaft, which ultimately regulates the torque and speed to drive the vehicle in order to meet the requirements of different forms of operating conditions. Consequently, it is unfeasible to negate the occurrence of fluctuations in the motor's current when the gearbox malfunctions. This presents an opportunity to utilize the motor's electrical signals to identify system anomalies. Therefore, the paper carries out a study on the failure characteristics and fault diagnosis of an ELV gearbox powertrain based on the current signals of the motor. Firstly, an experimental test platform was constructed based on the structural principle of the powertrain of ELV models. Tooth wear was then induced in the gearboxes, and the current signals of the motor were analyzed under different states. The results demonstrate that the wear of gearboxes will result in discrepancies in the amplitude, variance, kurtosis and the characteristics of zero−crossing points of the current signals. These findings provide new ideas for electric vehicle ELV powertrain troubleshooting.

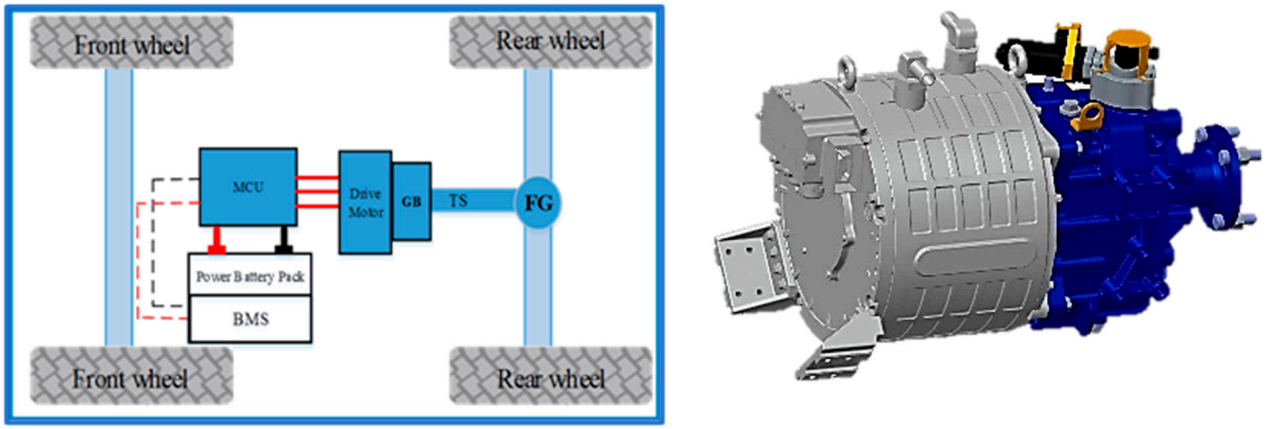
2. ELV Powertrain and Its Test Rig

This section provides a detailed analysis of the working principles and structural composition of the ELV powertrain. Understanding these foundational aspects is crucial for diagnosing and troubleshooting gearbox issues effectively. Based on the distinctive structural characteristics of the ELV powertrain, we have designed an experimental testing platform tailored specifically for this research.

2.1. Description of ELV Powertrain

As the core system of the ELVs, the powertrain works as the engine and transmission system of the traditional diesel or petrol−fueled vehicles (as shown in Figure 1). But in terms of energy conversion and power transmission, ELVs are different from traditional diesel or petrol vehicles. When an ELV is working normally, the electric energy stored in the battery system is first input to the motor controller, and then the motor controller inverts DC power into three−phase AC power. Finally, the electric energy is transformed to mechanical energy to drive the ELVs by driving the motor system. Conversely, when

the ELV is braking or slipping, the feedback energy will be stored in the battery system through the powertrain system. In order to further understand the ELV's powertrain system structure, the structure diagram of the ELV powertrain system is presented in Figure 1. Concisely, the functions of the components of the ELV powertrain system are listed as follows.



(**a**) (**b**)

Figure 1. ELV powertrain. (**a**) ELV powertrain structure. (**b**) ELV drive system.

As shown in Figure 1, the powertrain of an ELV has two main components, i.e., the drive motor and the gearbox. It is different from the connection of the traditional internal combustion engine car; the gearbox of the ELV's powertrain is directly connected to the drive motor in a coaxial series with a spline, and there is no flywheel mechanism. During vehicle operation, the motor controller controls the operating state of the drive motor and inputs the torque and speed to the gearbox through a mechanical rotor shaft, which ultimately adjusts the torque and speed to drive the vehicle to meet the vehicle's operation under different driving conditions. During the whole operation process, the motor controller can monitor the working status of the motor in real time through various types of sensors inside the drive motor (e.g., rotary position sensors, temperature sensors), etc., while the gearbox belongs to the purely mechanical components, and there are almost no corresponding sensors to monitor the fault conditions and working status. This leads to the fact that only when the gearbox is in complete failure or completely incapacitated can it be detected by the driver, and it is not possible to carry out preventive maintenance in advance, which, to a large extent, makes after−sales maintenance more difficult. In addition, in the ELV powertrain, the torque input from the motor first enters the input shaft gear for speed and torque adjustment, and finally it is output through the output shaft gear. In the working process, the output gear is directly connected to the drive shaft, which is susceptible to road conditions, and other complex environmental factors should be resulting in impact, vibration, etc., leading to more serious wear. This wear and tear can affect the motor's three−phase current signals to varying degrees, which provides a new method for the study of gearbox faults, and for this reason, it can be achieved by detecting the currents signals of the motor to detect faults in the gearbox.

2.2. Test Rig

In order to study and simulate the form of the current's signal characterization and fault characteristics of the ELV powertrain system gearbox failures under different operating conditions, the test rig that is specifically designed for conducting our study of the gearbox failure of ELV powertrain is shown in Figure 2.

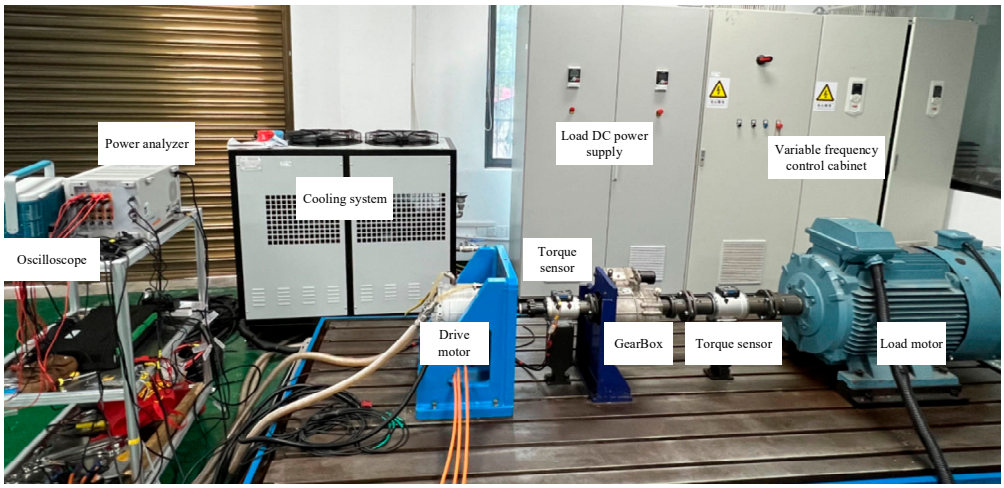


Figure 2. Test platform.

As shown in Figure 2, the specially designed gearbox of the ELV powertrain test rig comprises a host computer, monitoring software, power analyzer, oscilloscope, auxiliary power supply, cooling system, DC power supply, drive motor, variable frequency control cabinet, torque sensor, current sensor, fixed bracket, and other essential components. During testing, the host computer, in conjunction with the monitoring software, controls the entire test system's operation. It sends commands to the control unit via the CAN port and stores the information received from the control unit. The control unit serves as the intermediary, relaying commands from the host computer and collecting data from various components such as power analyzers, torque sensors, inverter cabinets, cooling systems, and motor controllers. Load motors simulate different operational loads, while torque sensors measure the torque and speed of the transmission chain. The frequency converter cabinet system powers the complete power system, and the cooling system ensures adequate cooling of the drive motors during operation. The power analyzer, connected to current and voltage sensors, analyzes the phase and distribution of the collected current and voltage signals and uploads these data to the host computer. The specific parameters and models of the components used in this test rig are detailed in the Table 1.

Table 1. Equipment specifications.

Specifications	Units	Values
Drive Motor		
Rated operational voltage	V	0~5
Maximum torque	A	0~10
Maximum power	Hz	1
Maximum speed	mS	10
Gearbox		
Maximum input torque	°C	−40–80
Maximum input speed	°C/min	0.1
Speed ratio	set	1
Power analyzer		
Max. sampling frequency	MS/s	2
Bandwidths	Hz	0.1 Hz~5 MHz
Sampling precision	A/V	5×10^{-4}
Operating temperature	°C	−20–65
Working voltage	V	AC220

3. Theoretical and Method

This section will focus on the theoretical approach used in this thesis. As illustrated in Figure 1, the motor and gearbox are directly connected in the ELV powertrain system. In the event of a failure of the gearbox, a torsional vibration signal will be generated. The torque output from the motor will exhibit periodic changes in conjunction with the torsional vibration of the gear, which in turn will result in alterations to the stator flux. Ultimately, this will lead to a specific regular change in the stator current. Therefore, by selecting electrical signals as the object of analysis and analyzing their characteristics after signal processing, it is possible to diagnose gear faults. The dynamic equations of the motor−drive system in the normal are

$$T_e - T_L = J\frac{dw_m}{d_t} + Bw_m \tag{1}$$

where T_e is the electromagnetic torque, T_Lr is the load torque, J is the motor moment of inertia, w_m is the motor speed and B is the friction coefficient. When the motor is in steady−state operation, the load torque T_L is constant; then, the w_m speed is also kept constant. Their balance equations are as follows.

$$\begin{cases} \frac{dw_m}{d_t} = 0 \\ T_e - T_L = Bw_m \end{cases} \tag{2}$$

When the motor cannot run smoothly due to the fault, the load torque T_L is not a constant value, and it will form an equilibrium state with a certain fluctuation law, until there is an oscillation difference for the periodic oscillation law to reach the equilibrium in the fault state, using the following formula.

$$\begin{cases} T_{e0} - T_{L0} = Bw_{m0} \\ T_{eosc} - T_{Losc} = J\frac{dw_{mosc}}{d_t} \end{cases} \tag{3}$$

Assuming that T_{Losc} satisfies the decomposition condition, further decomposition of T_{Losc} yields the following equation.

$$\begin{cases} T_e = T_e + T_{eosc} = T_{e0} + \sum_i T_{ei}\cos(2\pi f_i + \varphi_{ei}) \\ T_L = T_{L0} + T_{Losc} = T_{L0} + \sum_i T_{Li}\cos(2\pi f_i + \varphi_{Li}) \\ w_m = w_{m0} + w_{m0sc} = w_{m0} + \sum_i w_{mi}\cos(2\pi f_i + \varphi_{mi}) \end{cases} \tag{4}$$

where T_{L0} is the load torque; T_{e0} is the electromagnetic torque; w_{m0} is the average value of the rotational speed; T_{Losc}, T_{eosc} and w_{m0sc} are fluctuation constants for the mean values of load torque, electromagnetic torque and rotational speed, respectively; f_i is the frequency component in the Fourier spectrum in the oscillatory variable, T_{Li} is the peak of the shocks in the spectrum in the oscillatory component of the load torque, T_{ei} is the peak of the shocks in the spectrum in the oscillatory component of the electromagnetic torque; and w_{mi} is the peak shock of the spectrum in the oscillatory component of steady speed. φ_{ei}, φ_{Li}, and φ_{mi} are the phases of the load torque, the electromagnetic torque and the frequency components of the oscillating variables at steady−state speed, respectively.

For the motor when it is at a certain speed, according to motor control theory, it is known that the electromagnetic torque for $i_d = 0$ is

$$T_e = k_i i_q \tag{5}$$

where k_i is the coefficient of T_e, which is obtained from the i_q equation

$$i_q = i_{q0} + \sum i_{q0}\cos(2\pi f_i + \varphi_{qi}) \tag{6}$$

where i_{q0} is the average value of the current in the q−axis direction, i_{qi} is the component amplitude of the oscillating component with frequency f_i, and φ_{qi} is the corresponding phase component.

Transforming i_q to the a–b–c three coordinate system, the corresponding equation is

$$\begin{cases} i_a = -i_q \sin(\theta) \\ i_b = -i_q \sin\left(\theta - 120^\circ\right) \\ i_c = -i_q \sin\left(\theta + 120^\circ\right) \end{cases} \tag{7}$$

The motor rotor phase is

$$\theta = \theta_0 + \int pw_{m0}t = \theta_0 + pw_{m0}t + \sum \frac{pw_{mi}}{2\pi f_i} \sin(2\pi f_i + \varphi_{mi}) = \theta_0 + 2\pi f_{e0}t + \theta_{ts} \tag{8}$$

where θ_0 is the initial phase of the rotor, f_{e0} is the frequency of the rotor angular velocity mean, and θ_{ts} is the modulation component of the angular velocity oscillation quantity. The instantaneous frequency of the current has a component that is consistent with the frequency of the component of the load torque fluctuation, which is combined with Equation (6) to obtain the expression of the motor stator phase current.

$$\begin{cases} i_\alpha = -i_q \sin(\theta) = -i_q \cos\left(\theta + 90^\circ\right) + \sum_i i_{qi} \cos\left(2\pi f_i + \varphi_{qi}\right) \cos\left(\theta + 90^\circ\right) \\ = i_{q0} \cos\left(2\pi f_{e0} + \theta_0 + \theta_0 + 90^\circ\right) + \frac{1}{2}\sum_i i_{qi}\{(cos\ \left(2\pi(f_i + f_{e0})t + \varphi_{qi} + \theta_{ts} + \theta_0 + 90^\circ\right) \\ + cos\left(2\pi(f_{e0} - f_i)t - \varphi_{qi} + \theta_{ts} + \theta_0 + 90^\circ\right) \end{cases} \tag{9}$$

Therefore, the oscillations of the load torque are reflected in the phase currents as amplitude and phase modulation. The amplitude modulation is equal to the convolution of the two signal spectra, which indicates that the gear faults contain both AC and torsional frequencies in the stator current components, and by analyzing the stator current components, it is possible to diagnose the faults in the gears. When a normal gear rotates, the meshing stiffness is a regular periodic fluctuating signal. This means that whether the gear is normal or malfunctioning, as long as the gear mesh occurs, there will always be a component of the load torque with the same frequency as the change in the meshing stiffness. In the event of a localized tooth failure in a gear, an impulse shock will be observed in the load torque at the instant of meshing at the point of gear failure.

The kurtosis of the signal is a statistical parameter reflecting the distribution characteristics of the random variable in the time domain factor, which is generally expressed in ku. According to the theory of the kurtosis coefficient, the larger the kurtosis value is, the more periodic shock components it contains, which are both fault information conducive to fault diagnosis. Kurtosis is a kind of dimensionless parameter. The parameter itself is only related to the impact signal. When the speed of the gear is being detected, the type and load−bearing situation are applicable to the parts of the surface spalling damage fault identification. The formula for calculating the kurtosis is as follows [37]

$$ku = \frac{1}{N}\sum_{i=1}^{N}\left(\frac{x_i - x}{\delta}\right)^4 = \frac{1}{\delta^4 N}\sum_{i=1}^{N}(x_i - \overline{x})^4 \tag{10}$$

where N is the number of individuals; δ is the standard deviation; and $\overline{x}$ is the mean.

Kurtosis values are highly susceptible to impulsive shocks and are therefore well suited to the detection of localized damage faults in gears. During the normal operation of a gear, the amplitude distribution of the current signal is found to be close to the standard normal distribution. In the event of a gear fault, a large−value impulse shock is generated in the current signal. As the fault becomes more serious, the probability density of the large−value impulse increases, resulting in a deviation from the normal distribution of the current signal amplitude. This, in turn, leads to a deviation of the normal curve and an increase in the crag value. Consequently, the greater the magnitude of a component, the more fault−specific information it contains.

The variance is employed to delineate the extent of the signal's fluctuation, indicating the strength of the alternating current (AC) component of the signal. This is achieved by quantifying the average power of the AC signal, which is expressed as [37]

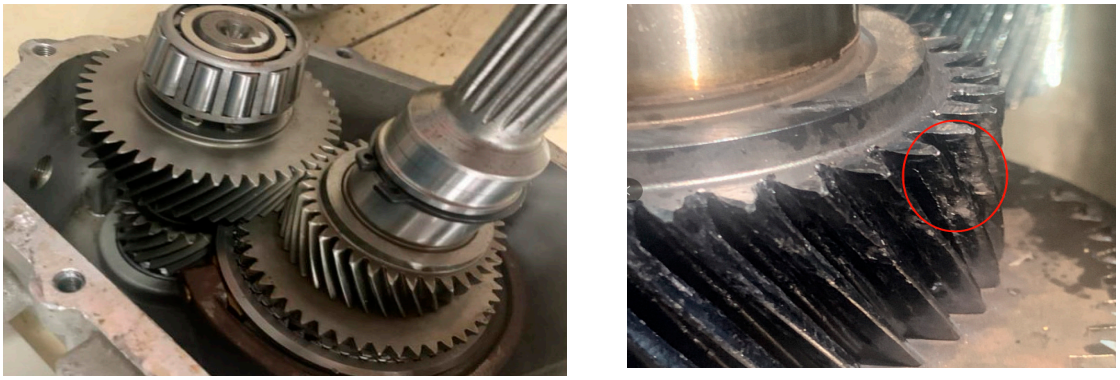
$$\begin{cases} S^2 = \frac{1}{n-1}\sum_{i=1}^{n}(x_i - \overline{x})^2 \\ S^2 = \frac{1}{n}\left[(x_i - \overline{x})^2 + (x_2 - \overline{x})^2 + \ldots + (x_n - \overline{x})^2\right] \end{cases} \tag{11}$$

Analysis of variance (ANOVA) is a statistical method used to analyze whether there is a significant difference in the means of three or more data sets. In gearbox troubleshooting, it can be used to determine whether a component is currently at fault by collecting and analyzing data from different operating conditions and comparing the difference in data between normal operating conditions and one or more abnormal conditions.

From the above, we can see that when the gearbox fails, we can analyze the electrical signals of the drive motor connected to it to diagnose the problem. However, it is still unknown how these signals change when the fault occurs and what kind of signals are most practical for gearbox fault diagnosis. The next section of the paper will analyze the current signals of the faulty gearbox under different loads with different signal processing methods to investigate the current signal changes under different working conditions and the effectiveness of the different signal processing methods in the identification of faults in the faulty state of the gearbox.

4. Result and Discussion

In order to investigate the change in motor current signal in the ELV powertrain under the wear state of its gearbox, the paper takes the gearbox (its model is 2S310) produced by a company as the object of research, which has been used in batches in pure electric light trucks, and its structure is shown in Figure 3.



(**a**) (**b**)

Figure 3. Normal condition and abnormal condition of gearbox gears. (**a**) Normal condition of gearbox teeth. (**b**) Gearbox teeth are worn.

Before the test, we first emptied the gearbox lubricant through the bottom oil drain hole and disassembled the gearbox to carry out wear on the tooth surface of the input shaft gear (as shown in Figure 3b). Following the completion of the tooth surface wear treatment, the faulty gearbox was reinstalled on the test platform. The study of gear wear is primarily concerned with the tooth surface wear of the tested gearbox. In order to facilitate a comparative analysis, the normal state and faulty state of the gearbox were also tested and analyzed. Considering the actual working condition of the ELV and the performance of the test rig, the experiment tested the current signal changes of the gearbox under different working conditions under the state of tooth wear, using time–frequency domain analysis, amplitude analysis, variance analysis, kurtosis analysis, and the over−zero current signal feature to study its fault characteristics.

4.1. Time–Frequency Domain Analysis

Time–frequency domain analysis is a commonly employed fault diagnosis method. In order to explore the time–frequency domain state of the motor current signals under different fault states, we collected the drive motor signals of the phase current at a motor input speed of 1000 rpm with a torque of 20 Nm in the normal condition and the gearbox tooth wear conditions, respectively, as shown in Figure 4.

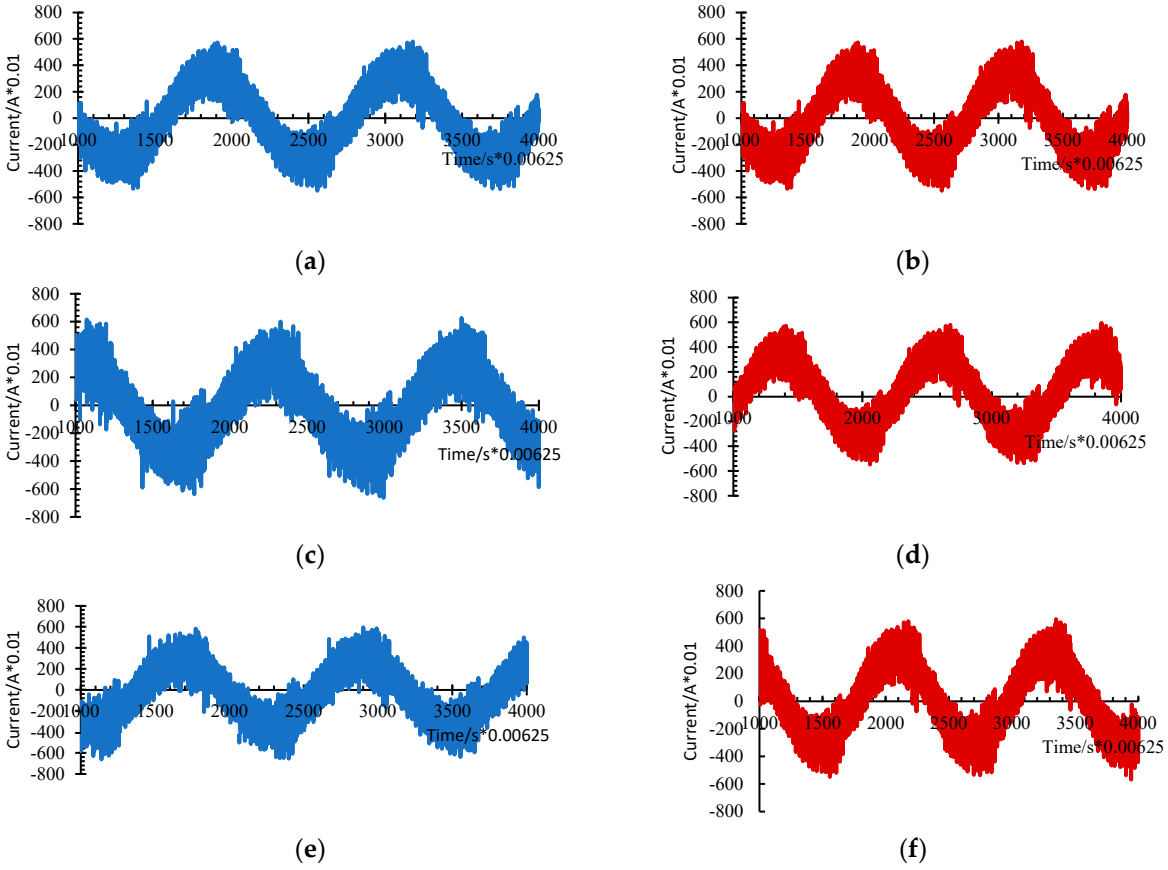


Figure 4. The phase current. (**a**) U−phase current when gearbox is abnormal. (**b**) U−phase current when gearbox is normal. (**c**) V−phase current when gearbox is abnormal. (**d**) V−phase current when gearbox is normal. (**e**) W−phase current when gearbox is abnormal. (**f**) W−phase current when gearbox is normal.

Figure 4 illustrates the phase current signals of the motor in the normal state and tooth wear state, respectively. According to this figure, it can be seen that there is no obvious difference between its time–domain analysis before and after the fault.

4.2. Analysis of Phase Current Signal Amplitude

The current amplitude signal of the motor is crucial, because they reflect the load and operational conditions of the gearbox. Variations in the amplitude of current signals can indicate abnormal wear or damage. During normal operation, the phase current signals maintain a consistent amplitude that corresponds to the standard load and mechanical efficiency of the gearbox. However, when gear wear or damage occurs, the current amplitudes exhibit irregular patterns and increased. Such changes in the signal can be detected through spectral analysis, which helps identify specific frequencies associated with faulty conditions. For this purpose, the maximum value of the U−phase current and the minimum value of the U−phase current were collected for a period of time under normal and damage conditions of the gearbox under different loads, as shown in Figures 5 and 6, respectively.

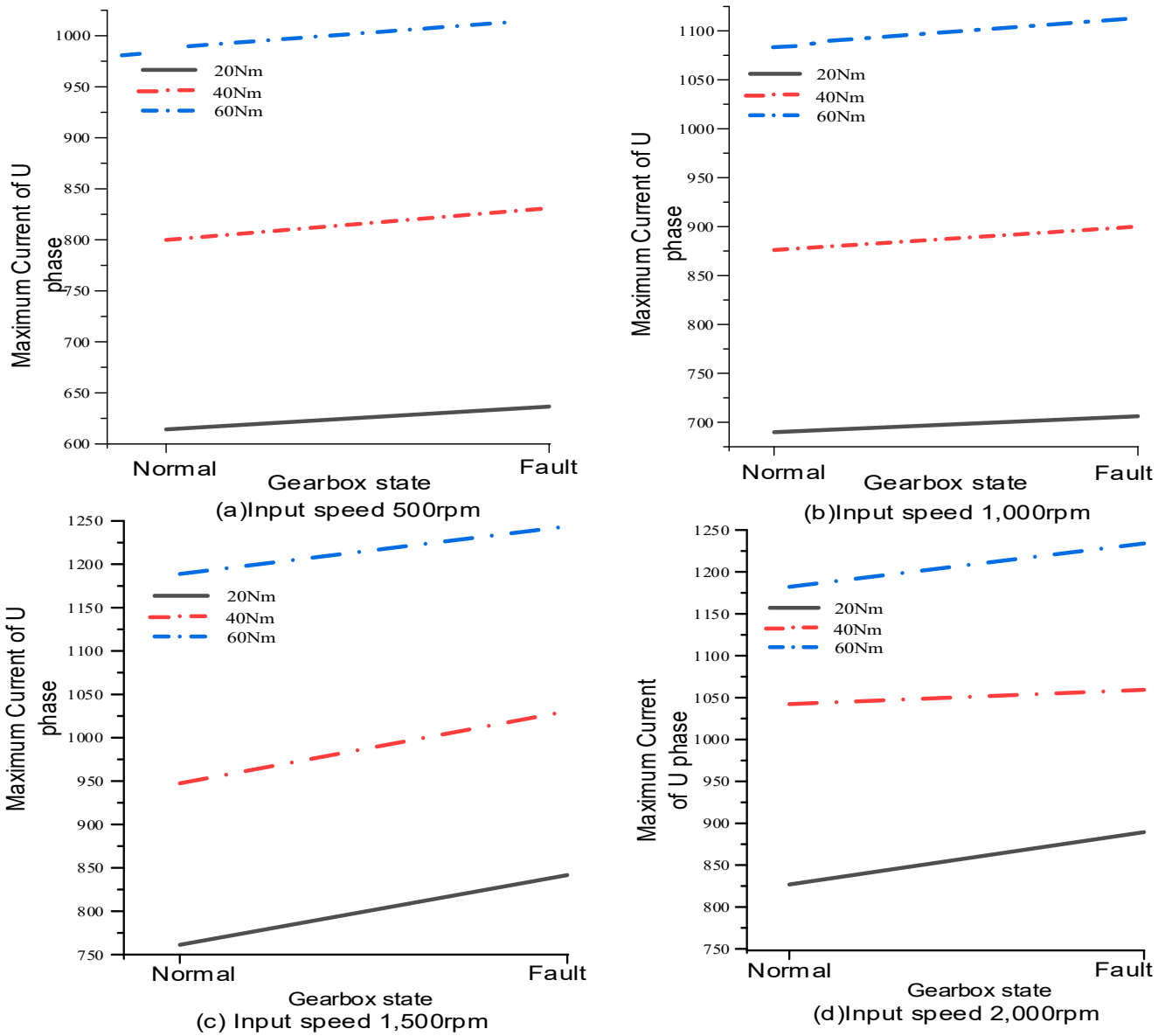


Figure 5. The average of the maximum values of the U−phase currents.

From Figure 5, it can be seen that the U−phase current increases with the increase in load regardless of whether the gearbox is in the normal or wear state. For example, at a speed of 1000 rpm and a load torque of 40 Nm, the peak current in the normal state is 8.75 A, and when the input torque reaches 60 Nm, the current is 10.8 A; in the same situation, when the gearbox teeth are worn, the peak current rises from 9.1 to 11.2 A. In addition, in all test conditions, gearbox tooth wear failure results in an increase in the peak motor current under identical load conditions. For instance, when the motor speed is 500 rpm and the load torque is 20 Nm, 40 Nm, and 60 Nm., the corresponding peak motor U−phase peak circuits are 6.12 A, 8.21 A, and 9.76 A, respectively; with peak currents increased by 0.25 A, 0.24 A, and 0.19 A, respectively, when the gears are faulty compared to peak currents under normal conditions. Similarly, when the load torque is 20 Nm, 40 Nm, and 60 Nm at 2000 rpm, the corresponding peak U−phase currents of the motor are 8.15 A, 10.46 A, and 11.75 A, respectively; and the peak U−phase currents increase by 0.28 A, 0.15 A, and 0.74 A, respectively, when the gear tooth surface fails.

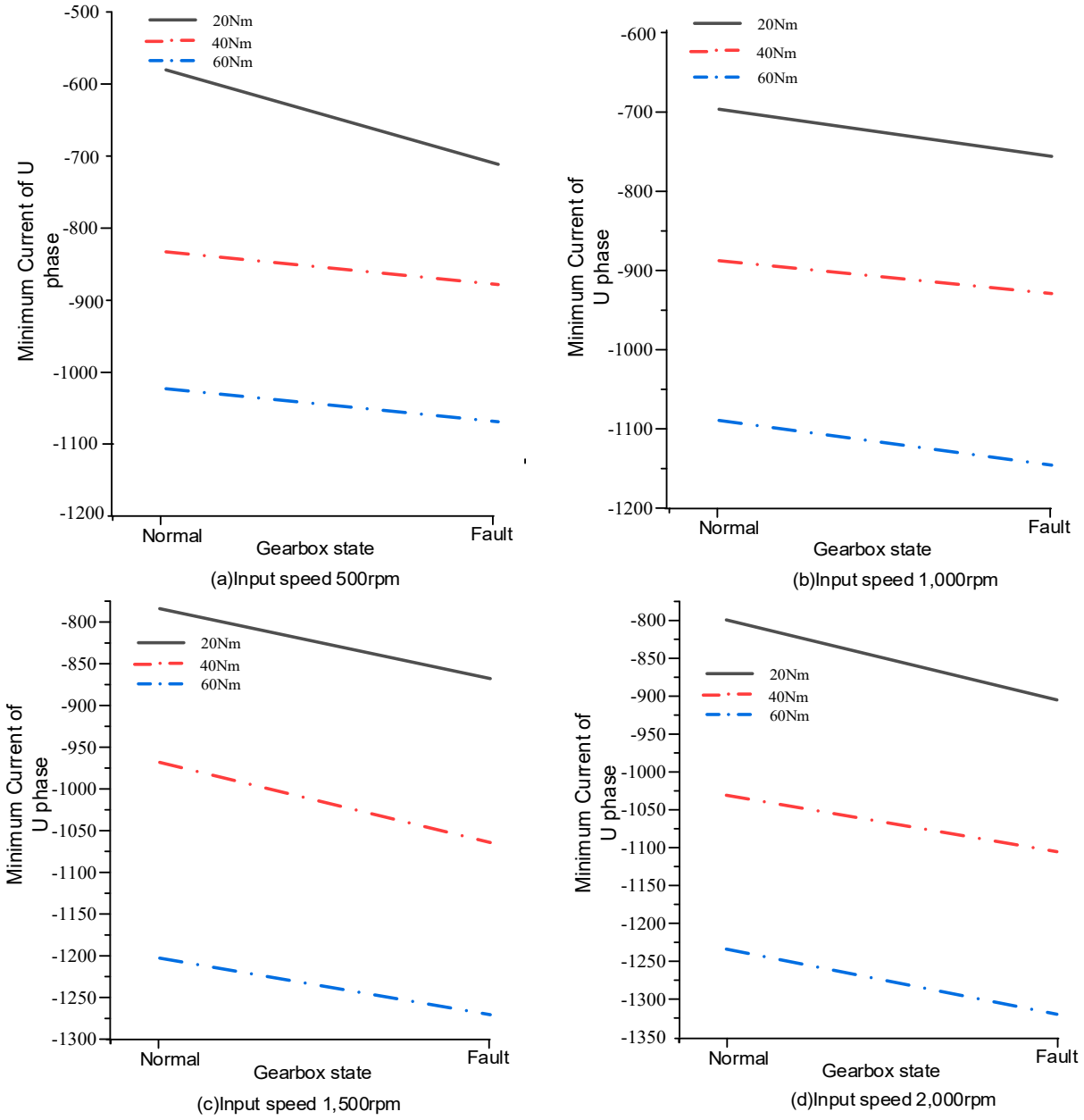


Figure 6. The average of the minimum values of the U−phase currents.

Figure 6 illustrates the mean values of U−phase current minima for the normal state and the state of gearbox tooth wear for different operating conditions. Similar to Figure 5, under the same load conditions, the gearbox tooth wear faults lead to an increase in the peak motor current assignments, which in turn makes the minima smaller. For example, when the torque is 20 Nm, 40 Nm, and 60 Nm, respectively, with a speed of 500 rpm, the corresponding peak motor U−phase peak currents are −5.92 A, −8.10 A, and −10.12 A, respectively. After gear wear, the peak currents are −1.62 A, 0.28 A, and 0.20 A, respectively, which are less than those in the normal state. When the motor speed is 2000 rpm and the load torque is 20 Nm, 40 Nm, and 60 Nm, the corresponding peak motor U−phase peak currents are −7.68 A, −10.61 A, and −12.25 A, respectively. These peak currents are reduced by −0.31 A, −0.21 A, and −0.25 A, respectively, compared with those of the normal state after the gear failure. This result is consistent with the theoretical study in the previous section.

4.3. ANOVA of Phase Current Signals

Variance in the current signals of drive motor is a sensitive indicator of operational inconsistencies and mechanical abnormalities in the gearbox. A stable gearbox operation typically shows low variance in the current signals, indicating uniform mechanical efficiency and load handling. When there is wear or damage in the gearbox, such as a misalignment of gears or degradation of gear teeth, the variance in current signals increases significantly. This increase is due to the uneven load distribution and increased friction within the gearbox. By conducting a statistical analysis of the variance in these signals, we can pinpoint deviations from normal operational parameters. This method allows for the early detection of potential problems, facilitating timely maintenance interventions. Monitoring and analyzing the variance of these signals not only helps predict imminent failures but also aids in optimizing the maintenance schedule, thus reducing unplanned downtime and improving the overall reliability and longevity of the gearbox systems. In order to achieve this objective, we collected the U−phase current signals with the intention of analyzing the ANOVA over a period of time in both the normal and wear states of the gearbox under different loads. The results of this analysis are presented in Figure 7.

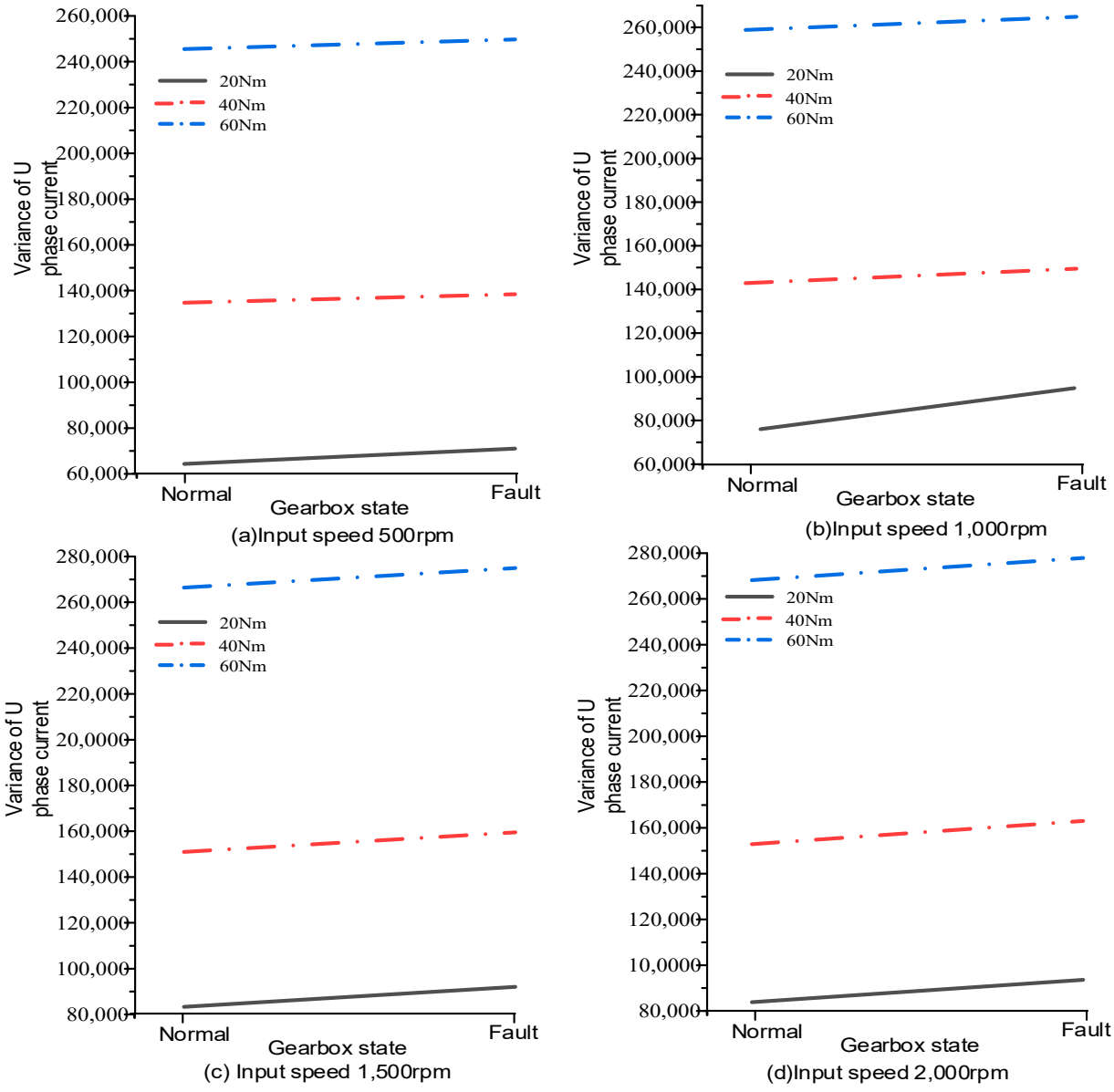


Figure 7. Variance of U−phase current.

From Figure 7, it can be observed that regardless of whether the gearbox is in a normal state or in a worn state, the U−phase current variance increases as the load increases. For instance, in the normal state, when the drive motor speed is 1500 rpm and the torque is 20 Nm, 40 Nm, and 60 Nm, the variance values are approximately 80,560, 14,980, and 260,522, respectively. Furthermore, the rotational speed exerts a relatively minor influence on the variance. To illustrate, when the speed is 500 rpm, 1000 rpm, 1500 rpm, and 20,000 rpm, respectively, with a load torque 40 Nm, the corresponding variance values are 78,600, 79,860, 80,260, and 80,658, which exhibit minimal variation.

4.4. Kurtosis Analysis of Phase Current Signals

Kurtosis, a statistical measure, is particularly valuable for identifying sharp peaks in signal distributions, which are indicative of abrupt changes in gearbox conditions. In a normally functioning gearbox, the kurtosis of the current signals should be relatively low, reflecting the uniformity and smooth operation of the gearbox mechanisms. An increase in kurtosis means the presence of sudden, non−standard fluctuations in the signal, which can be symptomatic of issues such as gear tooth breakage or severe misalignment. This sharp increase in kurtosis can be detected through signal analysis, where higher values indicate more pronounced deviations from normal gearbox behavior. By analyzing the kurtosis of the current signals, we can anticipate severe mechanical issues before they lead to catastrophic failure, thus enhancing the reliability and efficiency of gearbox operations in industrial settings. For this purpose, we respectively collected the U−phase current signals for crag analysis under normal and wear states of the gearbox under different loads, and the results are shown in Figure 8.

From Figure 8, we can see that regardless of whether the gearbox is in a normal or worn condition, the kurtosis of the U−phase current signal decreases with the increase in the load. This is in contrast to the signal of the phase current signal amplitude in Figure 5. For example, when the motor speed is 1500 rpm with a load torque of 40 Nm, the kurtosis value of the U−phase current is 2.16 when the gearbox is normal, and the value increases to 2.26 when wear occurs on the tooth surface. A comparable phenomenon is observed at other speeds of 500 rpm, 1000 rpm, and 2000 rpm. This shows that kurtosis analysis of phase current signals provides better diagnosis of gearbox models.

4.5. Characterization of Phase Current Signal Zero−Crossing Point

The analysis of zero−crossing characteristics in phase current signals from motors connected to the gearbox serves as a crucial diagnostic tool for identifying gear face wear and other mechanical issues. Zero−crossing points, which occur when the current signal transitions from positive to negative polarity or vice versa, are highly sensitive to mechanical irregularities within the gearbox. In a normally functioning gearbox, these zero crossings follow a predictable pattern, reflecting the regular operation and alignment of the gears. Deviations from this expected pattern can indicate mechanical problems such as gear tooth wear or damage, which disrupt the smooth transmission of power and introduce irregularities into the current signal. By monitoring and analyzing these zero−crossing features, it is possible to detect subtle changes in gearbox behavior that may not be evident through other signal characteristics. For this study, we collected U−phase current signals to perform zero−crossing point analysis under both normal and worn states of the gearbox across different load conditions. The results of this analysis are presented in Figure 8, demonstrating the efficacy of this method in diagnosing gearbox faults through phase current signal examination.

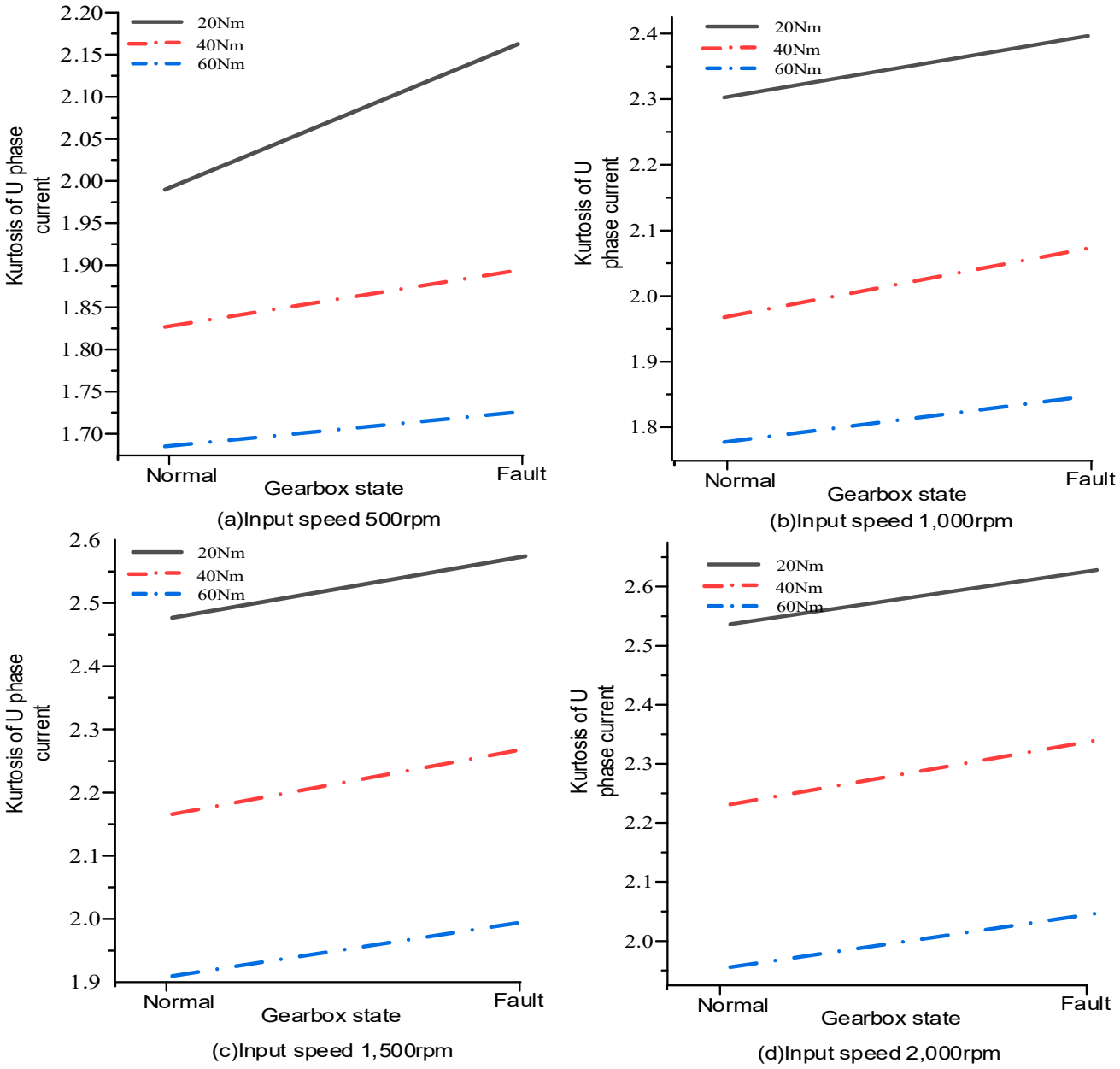


Figure 8. Kurtosis of U−phase current.

From Figure 9, we can see that the zero−crossing point of the U−phase current signal is influenced not only by the load but also by the fault state of the gearbox. For instance, when the gearbox is normal, and the load torque is 20 Nm, 40 Nm and 60 Nm with the speed of 1000 rpm, the U−phase zero crossing time is 0.0056 s, 0.0145 s and 0.0165 s, respectively: the U−phase zero−crossing time increases gradually with the increase in the load. In addition, the wear of the tooth surface will also lead to a change in the U−phase zero−crossing time, which will result in the time of the zero crossing being significantly smaller. For example, when the motor speed is 1000 rpm, and the load torque is 20 Nm, 40 Nm, and 60 Nm, the average time of the zero−crossing point of the U−phase current for gearbox tooth wear faults is 0.0042, 0.0119 s, and 0.0148 s, respectively.

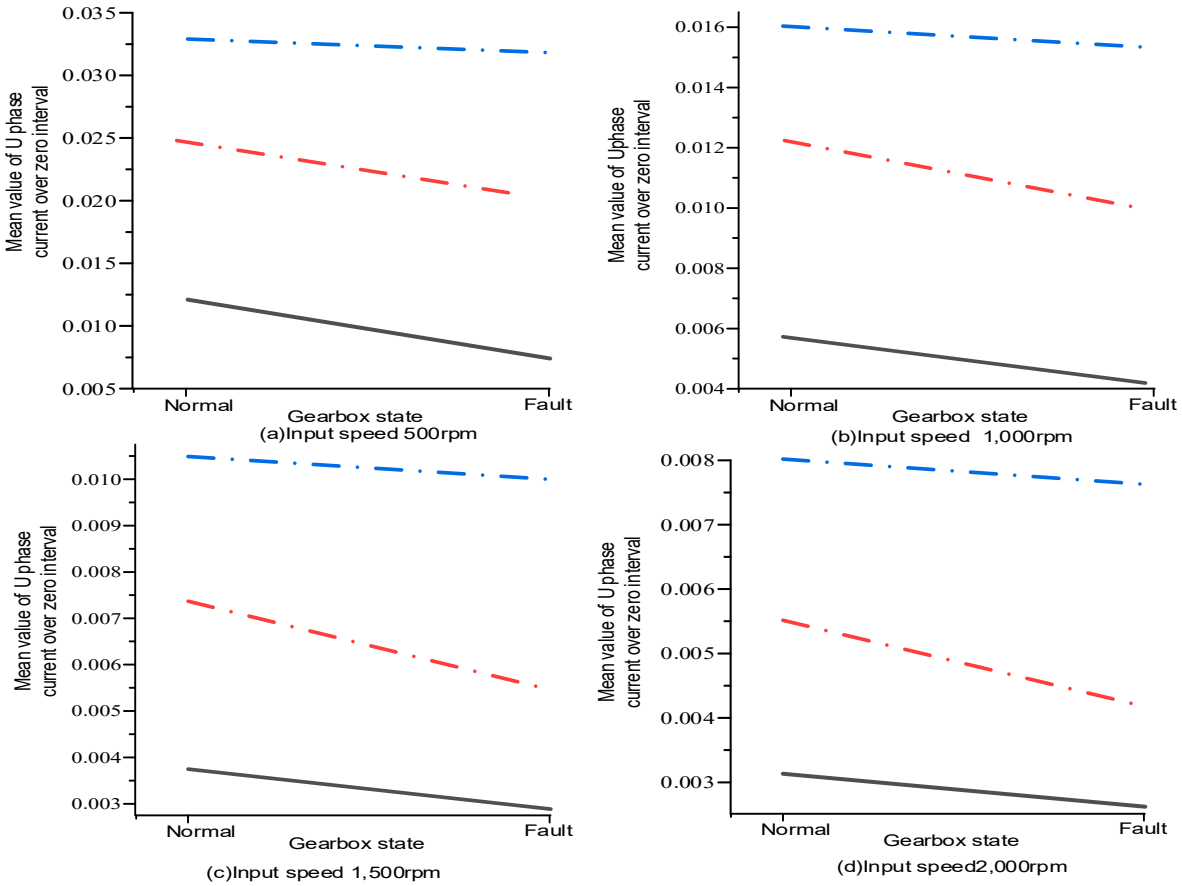


Figure 9. Mean value of U−phase current zero−crossing points.

The aforementioned study has revealed that when the gearbox fails, the characteristic information of gearbox tooth wear can be identified from the current signal to a greater extent through amplitude analysis, variance analysis, and kurtosis analysis. However, the detection results obtained by different analysis methods are inconsistent, and it is not known which method is more effective. For this reason, we have standardized the values of tooth flank wear under different working conditions and expressed them in percentage, as shown in Table 2.

From Table 2, it can be seen that when the gear tooth failure occurs, the maximum and minimum amplitude, variance, and crag value of the U−phase current signal increase, but the time required to pass the zero point gradually decreases, which is consistent with the test results of the above test. In addition, some signal characteristics are significantly higher than the average value: for example, when the input speed is not 1000 rpm and the input torque is 20 Nm, the variance after tooth wear is 16.5% of the normal variance, which is higher than the average value of 4.9%, which may be due to signal detection interference. Overall, when the gearbox fails, the amplitude of the current signal exceeds the normal condition by 4.6–4.7%, the variance of the current signal increases by 4.9%, the magnitude of the current signal increases by 5.2%, and the time to pass zero is about −5% of the normal condition. In comparison, crag analysis is more advantageous for gear tooth wear faults based on the current signal.

The findings from this research highlight the potential of using motor current signal analysis as a non−intrusive, cost−effective method for diagnosing gearbox faults in ELVs. The reliance on motor current signals, which are inherently monitored by most electrical systems, eliminates the need for specialized vibration sensors and reduces the complexity and cost of fault diagnosis systems. Moreover, the statistical parameters identified—amplitude, variance, kurtosis, and zero−crossing points—offer a robust framework for detecting and

characterizing gear tooth wear. These parameters can be integrated into advanced diagnostic algorithms, leveraging machine learning and artificial intelligence to enhance predictive maintenance capabilities.

Table 2. Changes in eigenvalues for different analysis methods after gearbox tooth failure.

Input Speed (rpm)	Load Torque (Nm)	Maximum Amplitude Analysis	Minimum Amplitude Analysis	Variance Analysis	Kurtosis Analysis	Zero−Crossing Analysis
500	20	4.7%	2.5%	4.4%	9.4%	−4.9%
	40	3.0%	5.8%	1.5%	4.7%	−7.3%
	60	3.5%	2.9%	3.1%	4.5%	−4.0%
1000	20	6.0%	8.7%	16.5%	4.8%	−10.9%
	40	3.4%	1.7%	1.3%	5.2%	−7.5%
	60	3.0%	5.9%	0.9%	4.8%	−1.9%
1500	20	7.5%	5.0%	7.9%	4.5%	−3.1%
	40	7.4%	4.6%	4.6%	5.2%	−4.2%
	60	2.9%	4.2%	2.3%	4.2%	−1.9%
2000	20	8.4%	5.0%	7.8%	5.0%	−3.2%
	40	1.1%	4.9%	7.3%	4.7%	−7.4%
	60	4.5%	4.5%	1.5%	5.1%	−3.7%
Average of analyzed results		4.6%	4.7%	4.9%	5.2%	−5.0%

Future research should focus on expanding the dataset to include a broader range of operating conditions and gearbox types, thereby improving the generalizability of the diagnostic models. Additionally, integrating these diagnostic methods with real−time monitoring systems could provide continuous health assessment of the powertrain, allowing for timely maintenance actions and preventing catastrophic failures. Implementing such advanced diagnostic tools can significantly improve the operational reliability and lifespan of ELVs, contributing to the sustainability and economic viability of electric logistics solutions. As the technology evolves, further enhancements in sensor accuracy, data processing speed, and machine learning algorithms will likely provide even more precise and actionable insights into gearbox health, driving the next generation of maintenance strategies in electric vehicle fleets.

5. Conclusions

With the increasing global emphasis on achieving net−zero targets, the Electric Logistics Vehicle (ELV) market has experienced significant growth over the past decade. The gearbox, as a crucial component of the ELV powertrain system, plays a vital role in ensuring the reliability and stability of ELV operations. In order to understand the effect on the motor phase currents after a wear failure of the variable speed tooth flanks in the powertrain, this paper carried out research on current signal−based electric vehicle powertrain gear tooth wear fault diagnosis. Through conducting this research, we obtained some important conclusions, which are outlined below.

(1) Gear tooth wear in the ELV drivetrain system leads to significant changes in the associated drive motor current signals. These changes are primarily observed in the amplitude, variance, kurtosis, and mean value of the U−phase current zero−crossing points. This indicates that current signal analysis, particularly focusing on these statistical parameters, can be a reliable method for detecting gear tooth wear.

(2) Even the gearbox loading and tooth wear both affect the amplitude, variance, kurtosis and mean value of phase current zero−crossing points, but not in the same way. For example, both increased load and gear tooth wear cause the phase current amplitude to rise, but while load increases lead to a decrease in kurtosis, tooth wear causes the amplitude to increase and the average zero−crossing value to decrease. This

distinction is critical for accurately diagnosing the root cause of anomalies in motor current signals.

(3) Under identical operating conditions, a gearbox failure results in the current signal amplitude exceeding the normal state by 4.6–4.7%, an increase in current signal variance by 4.9%, an increase in kurtosis by 5.2%, and a reduction in zero−crossing time by approximately 5% compared to the normal state. These quantitative changes provide a clear diagnostic criterion that can be used to identify and assess the severity of gearbox faults.

Author Contributions: X.S.: Methodology, supervision, and writing—original draft. Q.T.: Investigation, writing—original draft, and review and editing. K.Y., M.Z.: Conceptualization and validation. J.W.: Supervision and review. H.Z.: Testing and review. All authors have read and agreed to the published version of the manuscript.

Funding: The authors gratefully acknowledge the Science and Technology Foundation of Hunan Province (Grant No. 2023JJ50222, 2023GK2038, and 2022JJ50119), the National Key Research and Development Foundation (Grant No. 2022YFB3403200).

Data Availability Statement: Data are contained within the article.

Conflicts of Interest: The authors declare no conflicts of interest.

References

1. Chen, X.; Yang, Y.; Cui, Z.; Shen, J. Vibration fault diagnosis of wind turbines based on variational mode decomposition and energy entropy. *Energy* **2019**, *174*, 1100–1109. [CrossRef]
2. Shu, X.; Guo, Y.; Yang, W.; Wei, K.; Zhu, Y.; Zou, H. A Detailed Reliability Study of the Motor System in Pure Electric Vans by the Approach of Fault Tree Analysis. *IEEE Access* **2020**, *8*, 5295–5307. [CrossRef]
3. Zhang, B.; Li, X.; Zuo, Q.; Yin, Z.; Zhang, J.; Chen, W.; Lu, C.; Tan, D. Effects analysis on hydrocarbon light-off performance of a catalytic gasoline particulate filter during cold start. *Environ. Sci. Pollut. Res.* **2022**, *29*, 76890–76906. [CrossRef]
4. Shu, X.; Guo, Y.; Yang, H.; Zou, H.; Wei, K. Reliability Study of Motor Controller in Electric Vehicle by the Approach of Fault Tree Analysis. *Eng. Fail. Anal.* **2021**, *121*, 1–12. [CrossRef]
5. Sun, H.; Zi, Y.; He, Z.; Yuan, J.; Wang, X.; Chen, L. Customized multiwavelets for planetary gearbox fault detection based on vibration sensor signals. *Sensors* **2013**, *13*, 1183–1209. [CrossRef] [PubMed]
6. Yu, J.; He, Y. Planetary gearbox fault diagnosis based on data-driven valued characteristic multigranulation model with incomplete diagnostic information. *J. Sound Vib.* **2018**, *429*, 63–77. [CrossRef]
7. Qian, W.; Li, S.; Wang, J.; An, Z.; Jiang, X. An intelligent fault diagnosis framework for raw vibration signals: Adaptive overlapping convolutional neural network. *Meas. Sci. Technol.* **2018**, *29*, 095009. [CrossRef]
8. Singh, J.; Azamfar, M.; Ainapure, A.N.; Lee, J. Deep learning-based cross-domain adaptation for gearbox fault diagnosis under variable speed conditions. *Meas. Sci. Technol.* **2020**, *31*, 055601. [CrossRef]
9. Cheng, J.S.; Yu, D.J.; Yang, Y. A fault diagnosis approach for roller bearings based on EMD method and ar model. *Mech. Syst. Signal Process.* **2004**, *20*, 350–362.
10. Lei, Y.G.; He, Z.J.; Zi, Y.Y.; Hu, Q. Fault diagnosis of rotating machinery based on multiple ANFIS combination with GAs. *Mech. Syst. Signal Process.* **2006**, *21*, 2280–2294. [CrossRef]
11. Guo, J.C.; Shi, Z.Q.; Li, H.Y. Early fault diagnosis for planetary gearbox-based wavelet packet energy and modulation signal bispectrum analysis. *Sensors* **2018**, *18*, 2908. [CrossRef] [PubMed]
12. Park, J.; Hamadache, M.; Ha, J.M. A positive energy residual (PER) based planetary gear fault detection method under variable speed conditions. *Mech. Syst. Signal Process.* **2019**, *117*, 347–360. [CrossRef]
13. Kong, Y.; Wang, T.Y.; Chu, F.L. Meshing frequency modulation assisted empirical wavelet transform for fault diagnosis of wind turbine planetary ring gear. *Renew. Energy* **2019**, *132*, 1373–1388. [CrossRef]
14. Bajric, R.; Zuber, N.; Skrimpas, G.A. Feature extraction using discrete wavelet transformfor gear fault diagnosis of wind turbine gearbox. *Shock Vib.* **2016**, *2016*, 1–10. [CrossRef]
15. Cui, H.; Qiao, Y.; Yin, Y.; Hong, M. An investigation of rolling bearing early diagnosis based on high-frequency characteristics and self-adaptive wavelet de-noising. *Neurocomputing* **2016**, *216*, 649–656. [CrossRef]
16. Liu, Z.; He, Z.; Guo, W.; Tang, Z. A hybrid fault diagnosis method based on second generation wavelet de-noising and local mean decomposition for rotating machinery. *ISA Trans.* **2016**, *61*, 211–220. [CrossRef] [PubMed]
17. Magadán, L.; Granda, J.C.; Suárez, F.J. Robust prediction of remaining useful lifetime of bearings using deep learning. *Eng. Appl. Artif. Intell.* **2024**, *130*, 107690. [CrossRef]
18. Magadán, L.; Suárez, F.J.; Granda, J.C.; García, D.F. Low-Cost Industrial IoT System for Wireless Monitoring of Electric Motors Condition. *Mob. Netw. Appl.* **2023**, *28*, 97–106. [CrossRef]

19. Magadán, L.; Roldán-Gómez, J.; Granda, J.C.; Suárez, F.J. Early Fault Classification in Rotating Machinery with Limited Data Using TabPFN. *IEEE Sens. J.* **2023**, *23*, 24. [CrossRef]
20. Vasić, M.P.; Stojanović, B.; Blagojević, M. Fault Analysis of Gearbox in Opne PIT Mine. *Appl. Eng. Lett.* **2020**, *5*, 50–61. [CrossRef]
21. Vasić, M.; Stojanović, B.; Blagojević, M. Failure analysis of idler roller bearings in belt conveyors. *Eng. Fail. Anal.* **2020**, *117*, 104898. [CrossRef]
22. Vasić, M.; Blagojević, M.; Stojić, B.; Dizdar, S. Design and Performance Analysis of an in-wheel Hub reducer. *Adv. Eng. Lett.* **2022**, *1*, 115–125. [CrossRef]
23. Lee, J.; Azamfar, M.; Singh, J. A blockchain enabled Cyber-Physical System architecture for Industry 4.0 manufacturing systems. *Manuf. Lett.* **2019**, *20*, 34–39. [CrossRef]
24. Li, F.; Pang, X.; Yang, Z. Motor current signal analysis using deep neural networks for planetary gear fault diagnosis. *Measurement* **2019**, *145*, 45–54. [CrossRef]
25. Zhang, Y.; Ding, J.; Li, Y.; Ren, Z.; Feng, K. Multi-modal data cross-domain fusion network for gearbox fault diagnosis under variable operating conditions. *Eng. Appl. Artif. Intell.* **2024**, *133*, 108236. [CrossRef]
26. Pan, Y.; Zhang, L.; Wu, X.; Skibniewski, M.J. multi-classifier information fusion in risk analysis. *Inf. Fusion* **2020**, *60*, 121–136. [CrossRef]
27. Kia, S.H.; Henao, H.; Capolino, G.A. Analytical and experimental study of gearbox mechanical effect on the induction machine stator current signature. *IEEE Trans. Ind. Appl.* **2009**, *45*, 1405–1415. [CrossRef]
28. Bravo-Imaz, I.; Ardakani, H.D.; Liu, Z.; García-Arribas, A.; Arnaiz, A.; Lee, J. Motor current signature analysis for gearbox condition monitoring under transient speeds using wavelet analysis and dual-level time synchronous averaging. *Mech. Syst. Signal Process.* **2017**, *94*, 73–84. [CrossRef]
29. Zhang, R.; Gu, F.; Mansaf, H.; Wang, T.; Ball, A.D. Gear wear monitoring by modulation signal bispectrum based on motor current signal analysis. *Mech. Syst. Signal Process.* **2017**, *94*, 202–213. [CrossRef]
30. Chai, N.; Yang, M.; Ni, Q.; Xu, D. Gear fault diagnosis based on dual parameter optimized resonance-based sparse signal decomposition of motor current. *IEEE Trans. Ind. Appl.* **2018**, *54*, 3782–3792. [CrossRef]
31. Kia, S.H.; Henao, H.; Capolino, G.A. Gear tooth surface damage fault detection using induction machine stator current space vector analysis. *IEEE Trans. Ind. Electron.* **2014**, *62*, 1866–1878. [CrossRef]
32. Vashishtha, G.; Chauhan, S.; Kumar, S.; Kumar, R.; Zimroz, R.; Kumar, A. Intelligent fault diagnosis of worm gearbox based on adaptive CNN using amended gorilla troop optimization with quantum gate mutation strategy. *Knowl.-Based Syst.* **2023**, *280*, 110984. [CrossRef]
33. Wang, D. K-nearest neighbors-based methods for identification of different gear crack levels under different motor speeds and loads: Revisited. *Mech. Syst. Signal Process.* **2016**, *70*, 201–208. [CrossRef]
34. Su, Y.; Meng, L.; Kong, X.; Xu, T.; Lan, X.; Li, Y. Small sample fault diagnosis method for wind turbine gearbox based on optimized generative adversarial networks. *Eng. Fail. Anal.* **2022**, *140*, 106573. [CrossRef]
35. Wang, Y.-R.; Jin, Q.; Sun, G.-D.; Sun, C.-F. Planetary gearbox fault feature learning using conditional variational neural networks under noise environment. *Knowl.-Based Syst.* **2019**, *163*, 438–449. [CrossRef]
36. Liu, J.; Hu, Y.; Wang, Y.; Wu, B.; Fan, J.; Hu, Z. An integrated multi-sensor fusion-based deep feature learning approach for rotating machinery diagnosis. *Meas. Sci. Technol.* **2018**, *29*, 055103. [CrossRef]
37. Oppenheim, A.V.; Willsky, A.S.; Nawab, S.H. *Signals and System*; Publishing Housing of Electronics Industry: Beijing, China, 2020.

Disclaimer/Publisher's Note: The statements, opinions and data contained in all publications are solely those of the individual author(s) and contributor(s) and not of MDPI and/or the editor(s). MDPI and/or the editor(s) disclaim responsibility for any injury to people or property resulting from any ideas, methods, instructions or products referred to in the content.